

Thermo-economic assessment of reverse osmosis desalination system driven by the organic Rankine cycle

Zahra Hajabdollahi, Kyung Chun Kim*

School of Mechanical Engineering, Pusan National University, Busan 46241, Republic of Korea,
email: kckim@pusan.ac.kr (K.C. Kim)

Received 22 January 2019; Accepted 6 September 2021

ABSTRACT

A lack of fresh water can be observed in many countries with the increase of the world population. Therefore, waste heat was recovered from a diesel engine and used to run an organic Rankine cycle to supply power to a high-pressure pump, which pumps feed water to a reverse osmosis (RO) system. This study was done to increase the mass flow rate of fresh water production from the seawater. In order to increase the fresh water, a higher value of power is required which increases the total annual cost (TAC) of the system. The fresh water mass flow rate is defined as the efficiency of the system that increases by the increase of the power generated in the turbine. By considering the fresh water mass flow rate and cost as the two objective functions, an enhancement in one function destroys the other function. Due to the conflict between the functions, multi-objective optimization is required to apply to increase the thermal efficiency, and decrease the TAC. For these purposes, seven design parameters that some of the are turbine pressure, condenser pressure were selected, and a set of solutions were obtained for the optimized system parameters to find the effects of system design parameters on the system efficiency, TAC and consequently fresh water production. It was concluded that increasing the turbine pressure enhances the fresh water production, but increasing the condenser pressure decreases the mass flow rate of fresh water. In addition, increasing the feed water temperature and mass flow rate of feed water has positive effects on the RO recovery ratio and the mass flow rate of fresh water. Finally, a single solution is introduced as the final optimum point to evaluated different design parameter's effects on the system performance and fresh water production. The optimum magnitude for the system thermal efficiency was 37.99% with a TAC of 40,785 \$/y as well as 954.67 kg/s of fresh water.

Keywords: Reverse osmosis; Diesel engine; Organic Rankine cycle; Multi-objective optimization

1. Introduction

Water is one of the primary needs for every creature, and without it, life would be impossible. In order to provide fresh water, desalination is sometimes required. The desalination of saline water by reverse osmosis (RO) can be applied by an organic Rankine cycle (ORC) [1]. Many studies have presented a general concept of a desalination system that uses solar energy sources through the ORC to produce fresh water from the seawater. Solar collectors

combined with desalination technologies are critically reviewed [2]. A new hybrid system integrated with a photovoltaic (PV) to supply the system power was theoretically performed to increase the fresh water production with a low value of power consumption [3]. In their study, an average saving between 14.7% and 65% in power consumption was achieved.

A parabolic trough collector is applied to supply the heat for a steam turbine unit to generate electricity for running a RO [4]. The optimum configuration of the system was

* Corresponding author.

represented for the water and electricity production. It was concluded that maximum fresh water of 2,000 m³/d can be produced from the RO plant. Delgado-Torres and García-Rodríguez [5] suggested the design parameters of the solar ORC driven by a RO based on the energy consumed by RO and solar system efficiency [6]. It was shown that by the increase of the feed water temperature the consumed energy by the RO decreases. Karellas et al. [7] in a general analysis obtained 83,000 m³ of fresh water per year from a desalination system based on solar organic Rankine cycle (SORC). In an experimental research based on the RO and ORC, Manolakos et al. [8] found the fresh water production increases by the membrane pressure which consequently increases the water recovery. Shalaby [9] reviewed RO water desalination power plants run by PV and SORC systems. When energy recovery devices were used, preheating the feed water was not required. Delgado-Torres et al. [10] applied solar energy for fresh water production. They calculated the thermal efficiency of four working fluids and compared the results. Geng et al. [11] investigated the effects of feed water temperature rise on the total produced power of the ORC integrated with a RO in the cases of different mole fraction of R600/R601. It was resulted that the higher net power is generated in the case of R600/R601 (0.9/0.1). The effects of evaporator pressure on the total cost of the system and fresh water production unit cost were identified by Nemati et al. [12] in an ORC-RO system. By the increase of evaporator pressure the total cost of the system increases while the fresh water unit cost increases firstly and then increases. Igobo and Davies [1] constructed an ORC-RO machine in an experimental investigation using R245fa as the working fluid to evaluate the production of fresh water. Ibarra et al. [13] focused on the hourly analysis of the power and thermal efficiency of a desalination solar plants for 3 d selected in the winter and summer seasons separately, in which the water production was achieved to be 1.2 m³/h. In the a solar ORC-RO power plant by the increase of the ambient temperature the exergy efficiency of the system decreases [14].

In an ORC combined with the wind energy and the RO desalination the condenser temperature has an important impact on the daily output of fresh water [15]. The cost of different configurations of solar ORC-RO was compared with a basic system which showed that the turbine and pressure exchanger had the lowest investment and operating costs. The power required to run a RO process can be provided by applying solar energy in a heat-recovery steam generator. At a fixed feed water mass flow rate, increasing the salt concentration results in the maximum fresh water production at a lower temperature [16]. Carlos and Bicer [17] integrated a RO unit with a wind turbine and solar chimney as the prime movers and the effects of them were investigated on the thermal efficiency of the system and fresh water production. By application of solar chimney and wind the overall efficiency of the system was enhanced more as compared to the single solar chimney. Naseri et al. [18,19] developed a model to simulate a thermodynamic analysis of a cogeneration power plant for production of heat, hydrogen and water by application of a RO. They explored the effect of recovery ratio of RO on the water production and the rate of hydrogen production. A thermo-economic optimization of an ORC integrated with heat recovered by the diesel engine

was performed by Hajabdollahi and Kim [20] to increase the thermal efficiency of the system and decrease the cost, simultaneously. A thermo-economic simulation of a multi-generation system including Kalina cycle and desalination unit was performed by Ansarinassab et al. [21]. They found that using the stirling engine and magnetic cycles improves the combined systems. Ghamari et al. [22] designed a combined cooling, heat and power including a multi-effect desalination with thermal vapor compression and RO to enhance the thermal efficiency and the system cost.

No general research has focused on the thermo-economic aspect of a diesel-engine ORC integrated with RO desalination. Many studies were carried out on fresh water production as the only objective without considering the system's commercial status. The thermal efficiency of the system and total annual cost (TAC) reduction should be taken into account. In this work, a thermo-economic optimization of a diesel engine combined by an ORC is presented to produce power and fresh water from RO desalination. The working fluid of R245fa has been considered as the working fluid by the critical temperature of 154.01°C. The system efficiency was considered as one of the objective functions, which includes the thermal efficiency of the ORC, diesel engine, and RO desalination. The system's TAC was selected as the second objective function.

In the optimization problem the key factor is that to select the proper design parameters. After the selection of objective functions it is important to check which parameters have the highest effect on the both objective functions. It should be taken into account that these parameters should be independent from each other. As a result the design parameters are selected to be the evaporator pressure, condenser pressure, nominal capacity of the diesel engine, partial load, ORC mass flow rate, pump isentropic efficiency and turbine isentropic efficiency. For this purpose a multi-objective optimization algorithm was applied to maximize the total system efficiency and minimize the system TAC simultaneously. The most effective decision variables of the two objective functions were found using the distribution of each design parameter in the population generation. In the next step, the effects of the most effective design parameters on the TAC, efficiency, and the fresh water produced were found. The optimization and simulation code were written in MATLAB R2014b.

2. Thermal modeling

Fig. 1 shows a diagram of the ORC integrated with a RO unit and diesel engine. The waste heat produced by the diesel engine can be applied in an ORC-RO. The power produced by the ORC can be supplied in to a high pressure pump to pass the seawater to the RO desalination for the fresh water production purpose. In fact, the flow into the evaporator is heated and then passes through the vapor turbine to generate the power required to run the RO unit.

2.1. Turbine

The turbine inlet temperature can be determined using the heat recovered from the diesel engine via the evaporator as follows:

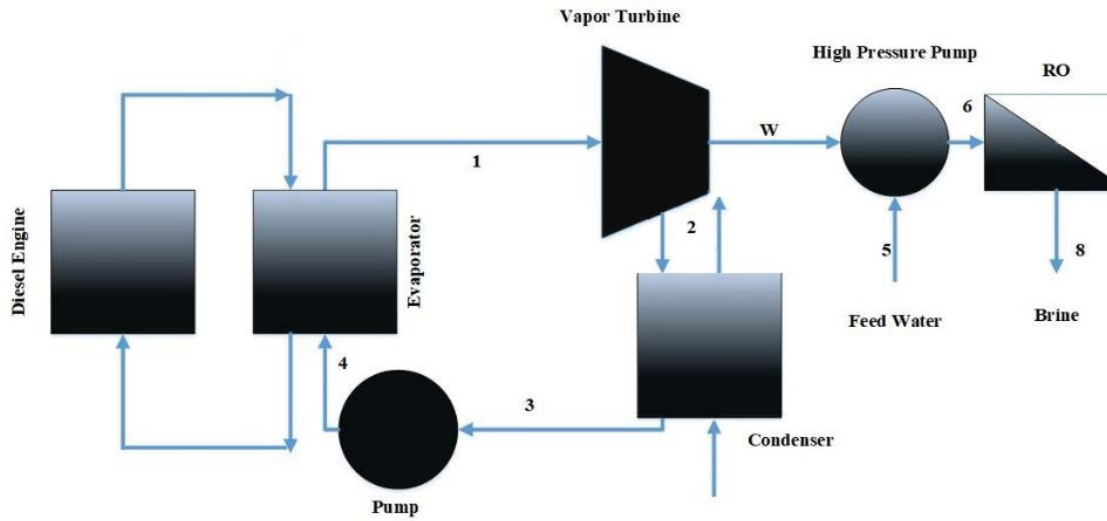


Fig. 1. A diagram of the ORC-RO unit.

$$T_1 = f(h_1, P_1), h_1 = h_2 \frac{Q_D}{\dot{m}} \quad (1)$$

where Q_D is the heat recovered from the diesel engine.

The thermal modeling of the equipment applied in the system was obtained by using mass and energy balance equations. The isentropic efficiency of the vapor turbine power in steady state is considered by neglecting the heat loss, as shown below:

$$\eta_T = \frac{h_1 - h_2}{h_1 - h_{2,s}} \quad (2)$$

where h is the specific enthalpy of the flow, and the subscript s represents the isentropic state. By having the pressure in point 1 the properties in point 2 are obtained by calculation of the isentropic properties in point 1. The power produced by the vapor turbine can be presented as:

$$W_T = \dot{m}(h_1 - h_2) \quad (3)$$

where \dot{m} is the ORC mass flow rate in the above equation.

2.2. Pump

The pump efficiency (η_p) applied in the ORC can be defined as follows:

$$\eta_p = \frac{h_3 - h_{4,s}}{h_3 - h_4} \quad (4)$$

Same as the vapor turbine by having the pressure in point 3, the properties in point 4 are obtained by calculation of the isentropic properties in point 3.

The power consume by the pump can be defined as:

$$W_p = \dot{m}(h_4 - h_3) \quad (5)$$

2.3. Condenser and evaporator

As shown in Fig. 1, a condenser and an evaporator are used for the condensing process and recovering heat from the diesel engine, respectively. The heat loss from the condenser as well as the evaporator is negligible compared with the exchanged heat. By applying the energy balance equation for the condenser we have:

$$\dot{H} = \dot{m}_h (h_i - h_o)_h = \dot{m}_c (h_i - h_o)_c = FUA\Delta T_{LM} \quad (6)$$

where \dot{m} , F , U , and A are the working flow rate, flow correction factor, overall heat transfer factor, and heat transfer surface area, respectively. Subscripts o , i , c and h represent the outlet, inlet state, cold and hot stream, respectively. ΔT_{LM} is logarithmic mean temperature difference (LMTD), which is expressed as follows:

$$\Delta T_{LM} = \frac{\Delta T_i - \Delta T_o}{\ln(\Delta T_i / \Delta T_o)} \quad (7)$$

where ΔT is the temperature differences between the hot and cold streams at the heat exchanger. Using this definition, LMTD for the condenser and regenerator are expanded as follows:

$$\Delta T_{LM,co} = \frac{(T_2 - T_{c,o}) - (T_3 - T_{c,i})}{\ln((T_2 - T_{c,o}) / (T_3 - T_{c,i}))} \quad (8)$$

By applying the energy conservation equation for the evaporator we have:

$$\dot{Q}_{eva} = \dot{m}(h_1 - h_2) \quad (9)$$

Finally, the outlet pressures of evaporator and condenser can be determined as follows by considering a constant pressure drop on each side of the equipment:

$$P_o = P_i(1 - \Delta P) \quad (10)$$

where P_i and P_o are the evaporator and condenser inlet and outlet pressure, and ΔP is the pressure drop.

2.4. Reverse osmosis desalination unit

In the RO units used for the desalination of brackish water, the water naturally flows osmotically from a lower concentration to a higher concentration. As shown in Fig. 1, the feed water enters the high-pressure pump powered by the ORC. The saline water enters the RO unit, and the non-ionic water molecules pass through the membranes, which have very small pores.

From the mass balance in the high-pressure pump, we have:

$$\dot{m}_5 = \dot{m}_6 \quad (11)$$

By applying the energy and mass balance equations for different equipment applied the following are obtained for the high pressure pump:

$$\dot{m}_5 h_5 + W_{p2} = \dot{m}_6 h_6 \quad (12)$$

$$\dot{m}_6 = \dot{m}_7 + \dot{m}_8 \quad (13)$$

$$\dot{m}_6 h_6 = \dot{m}_7 h_7 + \dot{m}_8 h_8 \quad (14)$$

The specific enthalpy of fresh water is obtained from a thermodynamic table, and in the cases of brine water, the equation below is used [23]:

$$h_b = 12.325 + \int_{T_0}^T (0.789 + (0.00279 \times (T - T_0))) dT \quad (15)$$

For the feed water and the brine water, the specific enthalpy is obtained as follows:

$$h = (1 - X) \times h_{\text{water}} + (X \times h_b) \quad (16)$$

where X and h_{water} are the salinity of the feed water and the specific enthalpy of the water without salinity obtained from the steam table. The brine water's mass flow rate is calculated as follows:

$$m_b = \frac{m_f \times (h_6 - h_7)}{h_8 - h_7} \quad (17)$$

where m_f and m_b represent the feed water's mass flow rate (equal to the mass flow rate of saline water at points 5 and 6) and brine water (produced at point 8).

The product mass flow rate (fresh water mass flow rate at point 7) is:

$$m_D = m_f - m_b \quad (18)$$

The feed water's mass flow rate is 2,500 kg/s, and its salinity is considered to be 0.1. The recovery ratio (RR) of the RO system can be obtained based on the mass flow rate of the feed water and fresh water:

$$RR = \frac{m_D}{\dot{m}_f} \quad (19)$$

The water salinity of the product can be calculated as follows:

$$X_p = \frac{((X_f \times m_f) - (m_b \times X_b))}{m_D} \quad (20)$$

where X_f and X_b are the salinity of the feed water and brine water, respectively.

The passage of salt through the membrane passage (the amount of salt that remains in the RO permeate after desalination) is defined as follows:

$$S_p = \left(\frac{X_p}{X_f} \right) \times 100\% \quad (21)$$

where X is the salt concentration in the product and feed water. The membrane salt rejection (S_r) is:

$$S_r = 100\% - S_p = \left[1 - \left(\frac{X_p}{X_f} \right) \right] \times 100\% \quad (22)$$

The nanofiltration membrane rejects less than 30% of the salt. The permeate flow rate through the RO membrane module was obtained from a previous study [24].

The membrane area is investigated as follows:

$$A_{m_p} = \frac{\dot{m}}{k_w} \times \frac{1}{\left(P_f - \frac{P_{cd}}{2} - P_p - \pi_{\text{cave}} + \pi_p \right)} \quad (23)$$

where π_p and π_{cave} are the osmotic permeate pressure and average feed side osmotic pressure, which can be calculated from:

$$\pi_p = \pi_f (1 - SR) \quad (24)$$

$$\pi_{\text{cave}} = \pi_f \times CP \times \frac{X_{fc}}{X_f} \quad (25)$$

X_{fc} , P_{cd} and CP are defined below:

$$X_{fc} = X_f \frac{\ln \left(\frac{1}{1 - RR} \right)}{RR} \quad (26)$$

$$P_{cd} = 0.01 \times n \times q_{\text{cave}}^{1.7} \quad (27)$$

where n represents the number of membranes, and q_{cave} is based on m_f and m_{brine} as follows:

$$q_{\text{cave}} = \frac{m_f + m_b}{2} \quad (28)$$

$$CP = \exp(0.7 \times RR) \quad (29)$$

2.5. Diesel engine

The diesel engine is applied as the prime mover (PM) with the nominal fuel consumption as follows:

$$m_{f-nom} = \frac{W_{nom}}{LHV \times \eta_{nom}} \quad (30)$$

where W_{nom} , η_{nom} and LHV are nominal power of the diesel engine, nominal efficiency of the diesel engine and lower heat value of the fuel. By calculation of the nominal fuel consumption, the fuel mass flow rate in the diesel engine is [25]:

$$m_f = m_{f-nom} \times \left(-0.02836 \times \exp^{0.03254 \times P_i} + 0.2556 \times \exp^{0.01912 \times P_i} \right) \quad (31)$$

P_i is presented to be the partial load. The efficiency based on the partial load can be generated in below:

$$\eta_{P_i} = \eta_{nom} \times \left(1.07 \times \exp^{-0.0005736 \times P_i} - 1.259 \times \exp^{-0.05367 \times P_i} \right) \quad (32)$$

The power and heat generated by the diesel engine are achieved from the curve fitting of the data vs. the partial load presented in reference [25] the power produced by the prime mover can be defined as follows:

$$W_D = \eta_{P_i} \times m_f \times LHV \times n_p \quad (33)$$

where n_p is the number of prime movers which is considered to be one in this study. Finally, the heat generated by the diesel engine is obtained as follows:

$$\frac{Q_D}{m_f LHV} = \frac{(24.01 \exp^{-0.0248 \times P_i} + 15.35 \exp^{0.002822 \times P_i}) + 0.001016 p_L^2 - 0.1423 p_L + 31.72}{100} - m_f C_p (T_{stack} - T_a) \quad (34)$$

where C_p is heat capacity which is considered to be 1.0035. Subscript a represents the ambient condition. Since the prime mover number is considered to be one, so it was not considered in the above equation.

2.6. Thermal efficiency

The total power produced by the cycle is the following:

$$W_{tot} = W_D + W_{ORC} \quad (35)$$

$$W_{ORC} = W_T - W_p \quad (36)$$

The total thermal efficiency of the system is defined as follows:

$$\eta_{tot} = \frac{W_{tot}}{m_f LHV} \quad (37)$$

where \dot{m}_f is the fuel required for the diesel engine, and LHV (kJ/kg) is the fuel's lower heating value.

3. Objective functions and constraints

Two scenarios were considered for the present study. In the first scenario, the fresh water produced by the RO unit and the total annual cost of the system were considered as objective functions. In the second scenario, the total efficiency of the system and the TAC were selected as the objective functions. Seven design parameters were chosen: the evaporator pressure, condenser pressure, nominal capacity of the diesel engine, partial load, ORC mass flow rate, pump isentropic efficiency and turbine isentropic efficiency.

The total power produced by the system was selected as a system constraint (first constraint). The condenser pressure must also be lower than the turbine pressure, and the condenser temperature must be higher than the ambient temperature (the second and third constraint). Finally, the vapor quality of the flow that exits the turbine is considered to be higher than 90% to avoid corrosion of the vanes (the fourth constraint).

3.1. Economic modeling of the system

In this study the thermal efficiency of the system is supposed to be maximized and the TAC is minimized. As a result, multi-objective optimization algorithm is implemented for this reason.

TAC is included with investment and operating cost. The investment cost is also included with capital cost (including the diesel engine, turbine, evaporator, RO unit, condenser, and pump) that are estimated based on the market available prices. The investment and fuel and emission costs are as follows [26]:

$$TAC(\$/year) = \alpha \beta C_{inv} + C_{fuel} + C_e \quad (38)$$

$$C_{fuel} = m_f \times t_{year} \times C_f \quad (39)$$

$$C_e = \dot{m}_{co_2} \times C_{po} \quad (40)$$

where \dot{m}_{co_2} , C_{po} and m_f are the mass flow rate of CO₂, emission cost in a year and fuel mass flow rate, respectively. t_{year} is the operational hours of diesel engine per year, and C_f is the fuel cost.

α is the annual factor and β is the maintenance factor, which is defined as follows:

$$\alpha = \frac{i}{1 - (1 + i)^{-n}} \quad (41)$$

where i is the interest rate of the system and n is the life time.

In this equation, the investment cost includes the cost of each piece of equipment used in the system. The equipment cost includes the prices of the diesel engine, turbine, evaporator, RO unit, condenser, and pump [27].

$$C_{inv} = C_{inv,T} + C_{inv,D} + C_{inv,RO} + C_{inv,eva} + C_{inv,con} + C_{inv,p} = a_1 (W_T)^{b_1} + a_2 (W_D)^{b_2} + a_3 (A_{Dis})^{b_3} + a_4 (A_{eva})^{b_4} + a_5 (A_{con})^{b_5} + a_6 (W_p)^{b_6} \quad (42)$$

The coefficients a_1 – a_6 and b_1 – b_6 are selected according to the local place.

4. Case study

R245fa was considered as the working fluid to run the ORC system. The ambient temperature was selected as 25°C. Feed water with a salinity of 0.1 passes through the high-pressure pump at a temperature of 36°C. The system was validated using previous results [14]. As it can be observed the present simulation results can be applied for the current system.

5. Results and discussion

This study was done to maximize the thermal efficiency of the system and decrease the TAC of an ORC combined with a diesel engine and RO desalination. NSGA-II code was written in MATLAB R2014b. The mutation and cross-over probabilities were assumed to be 0.035 and 0.85, respectively. The lower and upper bounds of variation are listed in Table 2. In the multi-objective optimization problems, a set of solution is always obtained as a Pareto front.

Fig. 2 shows TAC vs. the thermal efficiency of the system in the form of a Pareto front. Multi-objective optimization was carried out due to the trade-off between the TAC and efficiency. When increasing the thermal efficiency, the TAC is also increased. Therefore, the economic status of the system is important and has to be

considered as the second objective function. Five typical points were selected in the Pareto front to find the effects of the design parameters on the objective functions, as shown in Fig. 2. The highest efficiency was 38.5% with a TAC of 46,000 \$/y at point A. The lowest efficiency and TAC were achieved at point E. The points between B, C, and D have mediocre efficiency and TAC.

The distribution of the variables has calculated to find the parameters that have the highest effect on the trade-off between the TAC and efficiency, as shown in Figs. 3 and 4. The horizontal axis shown in Figs. 3 and 4 (Index) is the number of initial population that we have generated for the optimization algorithm. The partial load of the diesel engine and ORC mass flow rate have equal distributions through their bounds of variations. These two parameters have the highest effect on the trade-off between the TAC and efficiency. The turbine and condenser pressures and the turbine efficiency have semi-scattered distributions in their upper and lower ranges of variation. As a result, these parameters have mediocre effects on the trade-off behavior of the two objective functions (Fig. 2). The nominal capacity of the diesel engine and the pump efficiency have non-uniform distributions, which shows that they have the lowest effects on the TAC vs. the efficiency (Figs. 3b and 4d).

The effects of TAC vs. the efficiency are depicted in Fig. 5 for the five selected points shown in Fig. 2 at different partial loads. When increasing the partial load, the efficiency increases and then decreases, and the TAC increases regularly, which is not desired. When increasing the partial

Table 1
The validation of the results by the reference [12]

State number	Fluid	Temperature reference (°C)	Temperature present study (°C)	Specific enthalpy reference (kJ/kg)	Specific enthalpy present study (kJ/kg)	Mass flow rate reference (kg/s)	Mass flow rate present study (kg/s)
1	Isobutene	−27.8	−27.8	139.2	139.2	6	6
2	Isobutene	293.5	293.5	1,201	1,201	6	6
3	Isobutene	220	220	1,014	1,014	6	6
4	Isobutene	−28.4	−28.4	136.8	136.8	6	6
5	Saline water	36.2	36.2	146.7	145.7	2,500	2,500
6	Saline water	37.7	37.7	147.5	146.5	2,500	2,500
7	Brine	37.7	37.7	144.9	144.9	1,000	1,000
8	Fresh water	36.6	36.6	158.7	158	1,500	1,500

Table 2
Selected design parameters and their range of variations

Design parameters	Lower bound of variation	Upper bound of variation
Nominal capacity of diesel engine (kW)	50	200
Partial load (%)	40	100
Inlet pressure of turbine (kPa)	150	1,500
Outlet pressure of turbine (kPa)	10	1,500
ORC mass flow rate (kg/s)	0.3	5
Turbine efficiency (–)	0.5	0.9
Pump efficiency (–)	0.5	0.9

load, the waste heat from the PM increases, which increases the thermal efficiency of the ORC. From the other side, the power produced by the PM decreases at higher partial load that causes the thermal efficiency of the total system (ORC and diesel engine) to be decreased. In the higher thermal efficiencies, the effects of partial load increase is more significant on the reduction of diesel power. As a result, in the points A, B and C a decrease of efficiency is obtained by the increase of the partial load. As a result, there is an optimal point for the partial load where the thermal efficiency of the system is the highest in a specific value of partial load.

At a fixed TAC for the optimal solution of each point, the thermal efficiency of point A is the highest, followed by points B, C, D, and E. The black plus signs show the points that did not satisfy the limitations in section 3. The constraints are violated at lower efficiencies of the Pareto fronts at points D and E. Because of the lower partial load at lower efficiencies, the total power generated by the PM is decreased, which may violate the first constraint. The trade-off between the objective functions can be observed for the points where the constraints are satisfied because the efficiency decreases when increasing the partial load, and TAC increases (Fig. 3a).

Fig. 6 shows that the efficiency decreases and TAC increases when increasing the nominal capacity of the diesel engine. The nominal capacity of the diesel engine has the lowest effect on the trade-off behavior of the two objective functions, which is why both objective functions destroy when increasing the nominal capacity (which is also

shown in Fig. 3b). When increasing the nominal capacity, the useful power produced by the diesel engine increases, and consequently, the waste heat from the PM decreases. Therefore, the ORC's power production has more effect on the total efficiency of the system than the power generated by the PM, and the total thermal efficiency increases in the diagram. The fuel consumed by the diesel engine is also

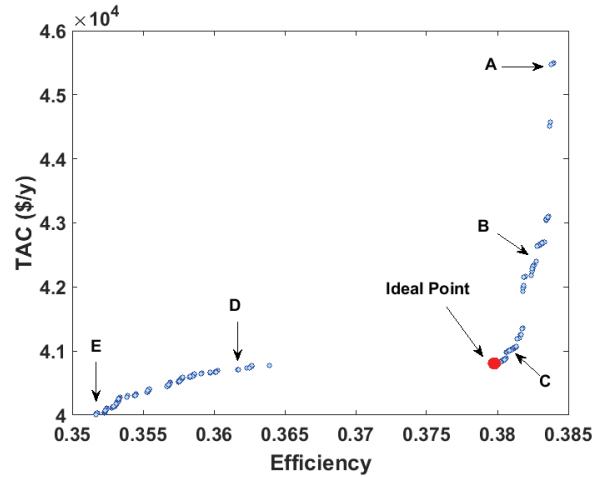


Fig. 2. Optimization Pareto front of total annual cost vs. efficiency.

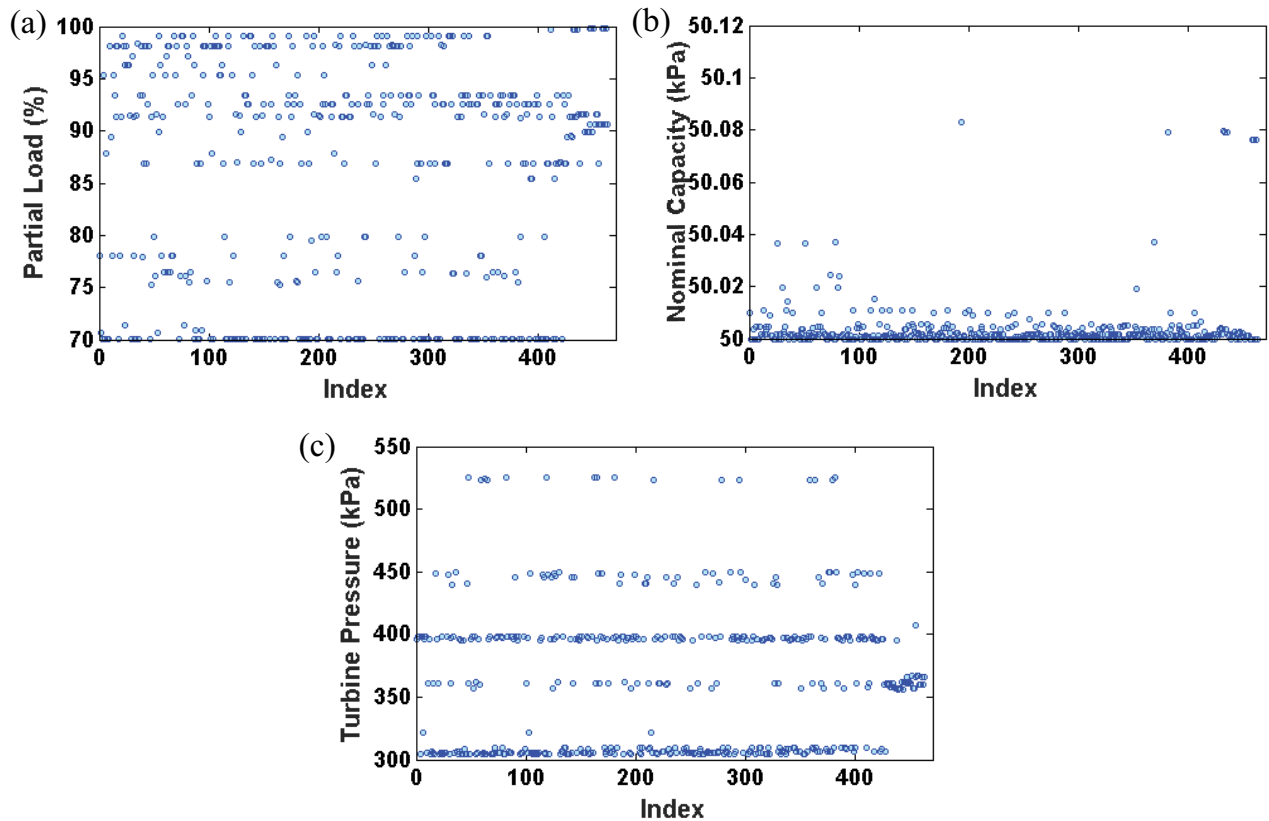


Fig. 3. Parameter distributions through their range variation: (a) partial load, (b) nominal capacity, and (c) turbine pressure.

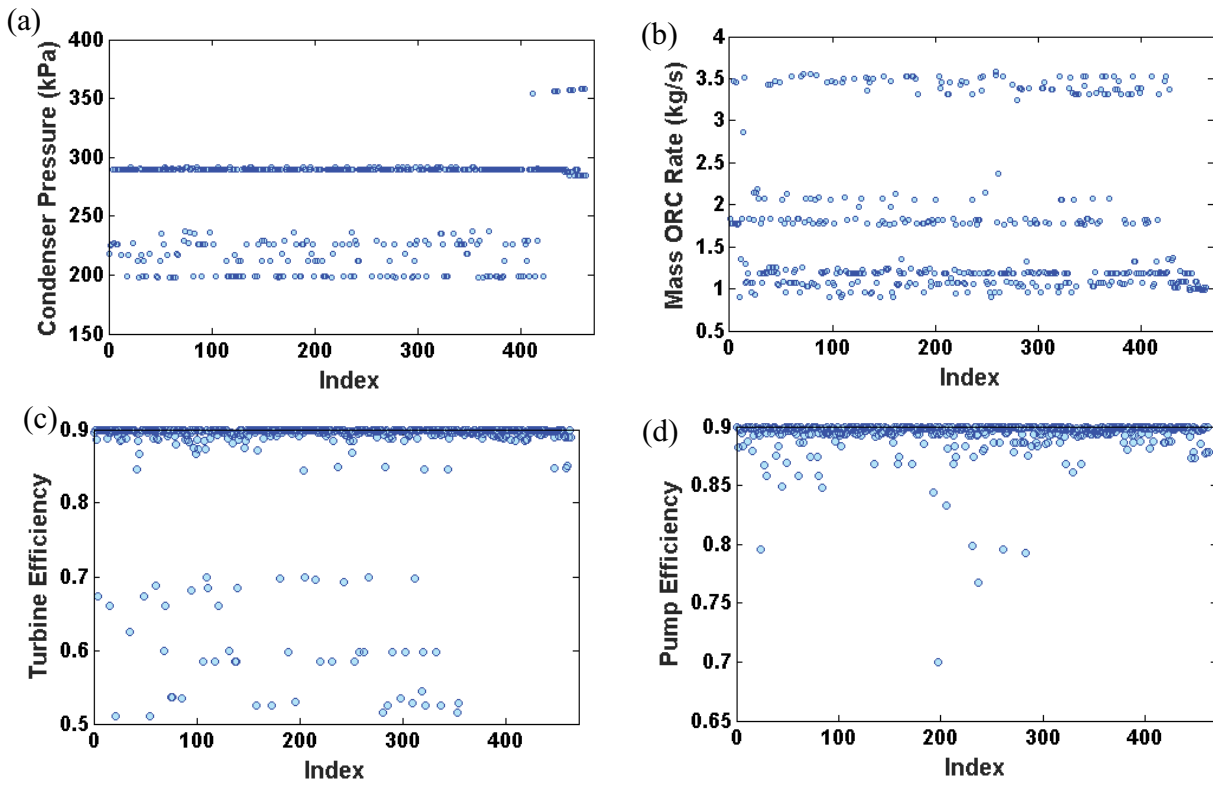


Fig. 4. Distribution of parameters via their upper and lower bounds of variation : (a) condenser pressure, (b) ORC mass flow rate, (c) turbine efficiency, and (d) pump efficiency.

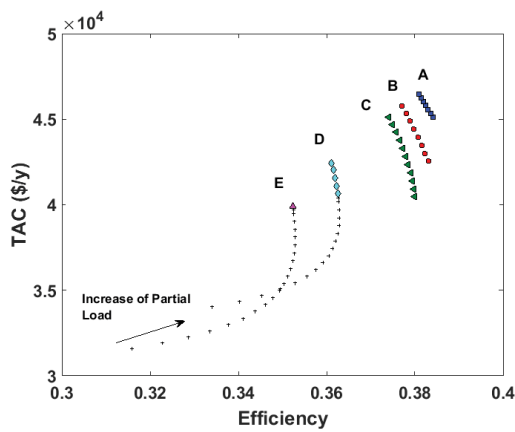


Fig. 5. Optimization Pareto fronts for the points selected in Fig. 2 at different partial loads.

increased, which causes a decrease in the overall system efficiency.

At lower efficiencies, the constraints are violated, as shown in Fig. 7 that happens in the lower turbine pressure. At lower turbine pressure, the working fluid temperature decreases, which causes the third constraint to be violated. At lower turbine temperature, there is less waste heat from the PM, and the power produced by the ORC decreases at lower efficiencies. Therefore, the first constraint in section 2 can be destroyed. When varying the turbine pressure, the

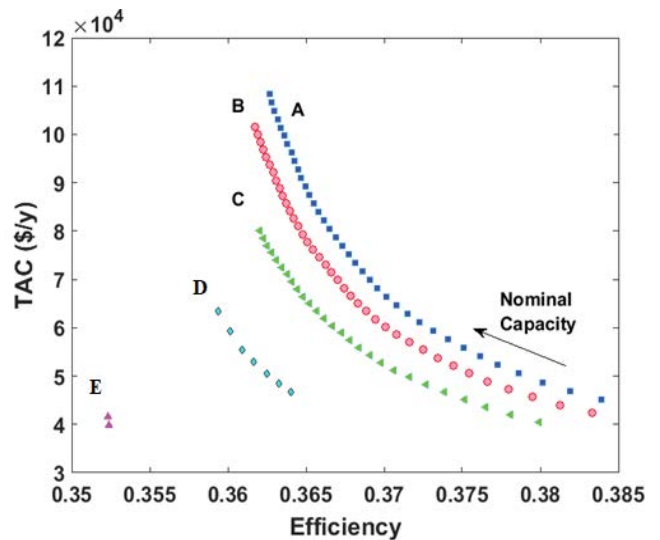


Fig. 6. Variation of objective functions for the points selected in Fig. 2 for different nominal capacities.

efficiency is highest in the case of point A and varies between 37% and 38.5%. The next highest is at point B, where the efficiency is between 37.2% and 38.3%. The results at points C and D are the next highest. The efficiencies are lowest in the case of point E and varied from 35.2% to about 37%. Thus, although the efficiency is highest at point A, the system cost

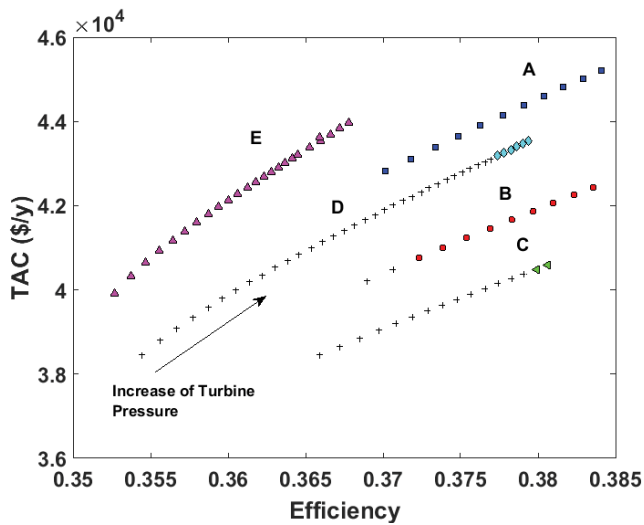


Fig. 7. Variation of total annual cost vs. the efficiency of the system at points selected in Fig. 2 for various turbine pressure.

is also very high. The results at point C can be considered more reasonable where the TAC and efficiency have the mediocre values. It is shown that the efficiency difference in the case of point C and point A (with higher efficiency) is not significant, but the cost difference is very high.

The opposite trend is shown in Fig. 8, where increasing the condenser pressure decreases the thermal efficiency and TAC. By increasing the condenser pressure, the condenser temperature increases and leads to a decrease in the efficiency. When the condenser pressure is higher, constraint 2 may be violated and the condenser pressure become higher than the turbine pressure. By decreasing the working fluid temperature, it means a less waste heat was received by the ORC. As a result, the power produced by ORC decreases too, and the first constraint may not be satisfied at a higher condenser pressure. The highest and lowest values of efficiencies are obtained by using the design parameters obtained in the points A and E, respectively. In the lower condenser pressure, the highest value of efficiency regarding the results for the point B is almost the same as the highest efficiency in the point A, but the TAC has the significant difference. TAC has about 5% decrease in the case of results presented on the point B as compared with the point A.

When increasing the ORC mass flow rate, the thermal efficiency increases, and at lower mass flow rates, the working fluid temperature of the ORC decreases, which can violate the third limitation, as shown by the plus signs in Fig. 9a. The highest efficiency is obtained in the point A and is followed by the points B, D, C and E, respectively. From the figure it is seen that by the increase of the efficiency, the system cost increases too. The highest and lowest cost is happened in the case of point A and point E, respectively. However the results associated with the point B have the higher efficiency than the results on the point D, but the cost of the point B is lower than the point D. As a result, the results associated with the point B can be introduced as the solutions that have the mediocre values of cos and

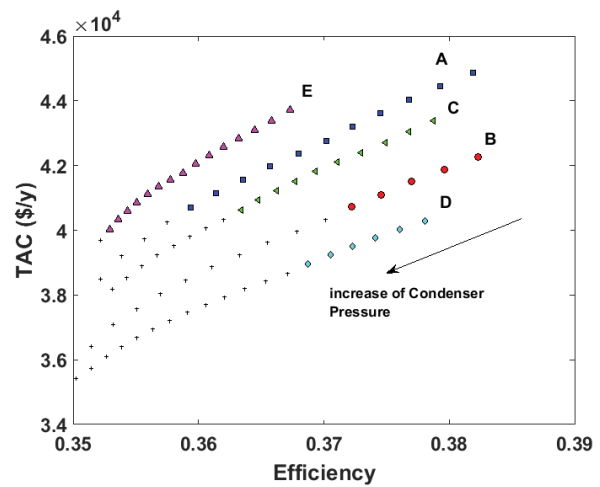


Fig. 8. Effects of condenser pressure on the optimized solutions of total annual cost vs. the thermal efficiency of the system.

efficiency. Fig. 9b shows the effects of the turbine efficiency on the variation of the TAC vs. the efficiency. When increasing the turbine efficiency, the power produced by the turbine increases and it causes an increase in the system efficiency. At lower efficiency of the turbine, the power produced by the turbine and the total power of the system decrease, and the first constraint may not be satisfied.

The pump efficiency has very little effect on the trade-off between the TAC and efficiency. Fig. 9c shows the results of varying the pump efficiency for the five selected points shown in Fig. 2. The best results are at point C, where the efficiency decreases by just 1.325% compared with point A, but the TAC has decreased 10.98%. In comparison with point E, which has the lowest TAC, there is a 7.95% increase in the efficiency of point C. There is also a 1.25% increase in the TAC at point C compared with point E.

Figs. 10–12 show the effects of different parameters on the production of fresh water. When increasing the nominal capacity, the increase in turbine temperature leads to an increase in the power production of the turbine. Thus, higher power can be supplied to the RO high-pressure pump which causes more seawater to be pumped and higher production of fresh water. Point A has the highest system efficiency (as shown in Fig. 2). This means that the turbine power is higher, which increases the fresh water production. The next best results occur at points B, C, D, and E. More fresh water is produced when selecting the design parameters related to point A. In contrast, the least fresh water is produced at point E.

When increasing the condenser pressure, the condenser temperature increases, as shown in Fig. 11. This occurs because lower power is generated by the turbine, which is why the turbine outlet temperature and condenser inlet temperature increase. Therefore, the lower turbine power leads to a decrease in the high-pressure pump power. Pareto front A dominated over the other Pareto fronts. This means that every point selected in Pareto A produces more fresh water at a fixed condenser pressure than the other Pareto fronts. The points at higher condenser pressure also destroy the results. At these points,

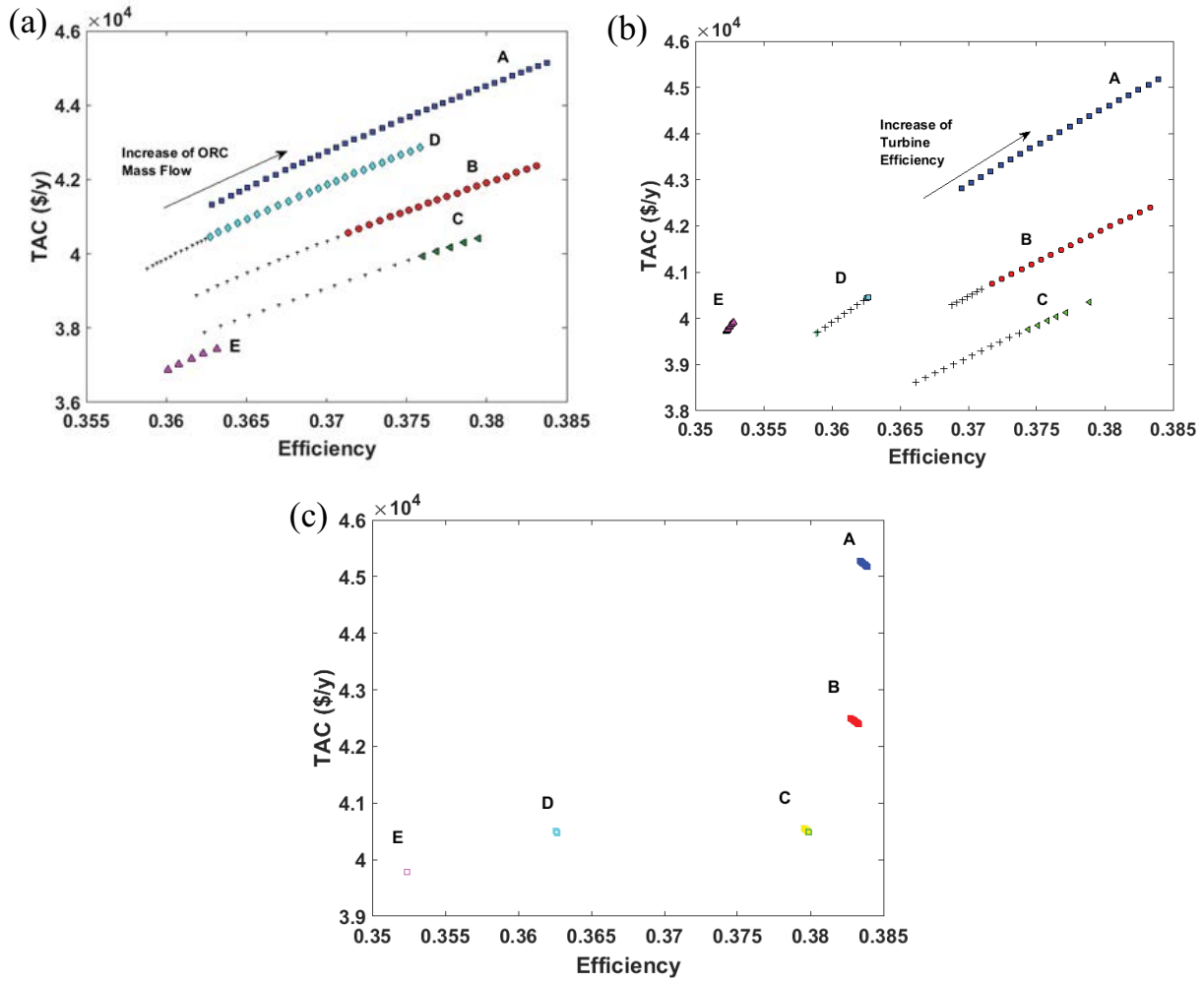


Fig. 9. The effects of total annual cost on the system efficiency with different parameters: (a) ORC mass flow rate, (b) turbine efficiency, and (c) pump efficiency.

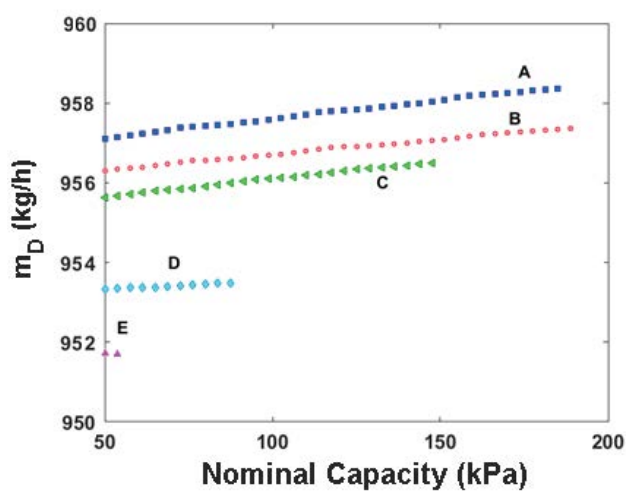


Fig. 10. Increase in fresh water mass flow rate at nominal capacity at the optimization points of the Pareto front.

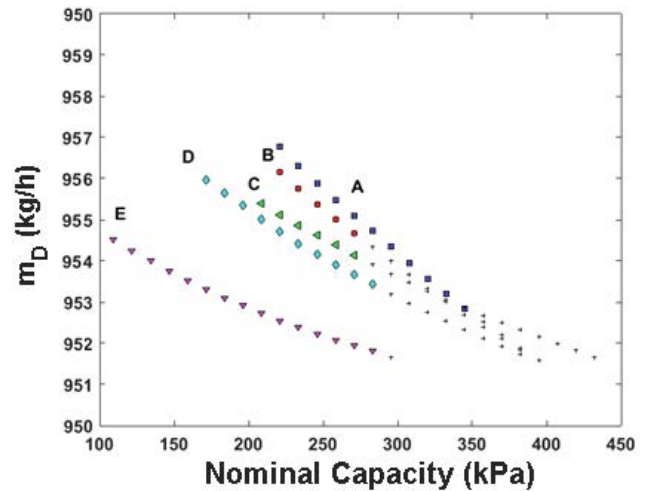


Fig. 11. Fresh water variation based on the condenser pressure at points A–E.

less fresh water is generated because of the lower ORC power, and as a result, the first constraint is not satisfied in this case.

Fig. 12 shows the variation of turbine efficiency and fresh water production for the five points shown in Fig. 2. The results at points D and E show that the turbine efficiency has a negligible effect on the fresh water production. This occurs because the distribution of the turbine efficiency is not scattered through its bound of variations for points D and E. However, at points A, B, and C, there is an increasing trend. Generally, increasing the turbine efficiency increases the fresh water produced.

The concept of the final optimum solution is presented to find the effects of different design parameters on the fresh water mass flow rate. For this purpose, the closest point to the ideal point shown in Fig. 2 is considered as the final solution. The LINMAP method is used as follows [28,29]:

$$d_i = \sqrt{\sum_{j=1}^2 (F_{ij}^n - F_{ideal,j}^n)^2} \quad (43)$$

where

$$F_{ij}^n = \frac{F_{ij}}{\sqrt{\sum_{i=1}^n (F_{ij})^2}} \quad (44)$$

In this relation, i is the index of each point on the Pareto front, j is the objective function index, and n is the total number of points in the Pareto front. The final point is considered as the final answer.

6. Final point

Based on the LINMAP method the point C is calculated to be the final optimum point. However the point A brings the highest efficiency but it is not considered as the final optimum answer. From the other side, the point E is also not considered as the final answer since it has the lowest efficiency (however it has the lowest cost as compared to the all points on the Pareto fronts). As a result, point C is calculated to be the final optimum answer since it satisfies both the objective functions reasonably.

The system parameters in the optimum final point are listed in Table 3. The system efficiency in the final optimum point has 1.05% decrease in comparison with the point A (thermodynamic optimum point with efficiency of 0.3839) while the TAC decreases 11.51% as compared with the point A (with TAC of 45,481 \$/y).

Fig. 13a shows the effects of turbine pressure on the mass flow rate of fresh water in different feed water mass flow rate for the final point. In fact, the different graph lines in the Fig. 13 are shown in the different feed water mass flow and its value is increased in the direction of the arrow. When increasing the turbine pressure, the output power increases. The increase of the feed water mass flow rate has a positive effect on the freshwater production. At a fixed condenser

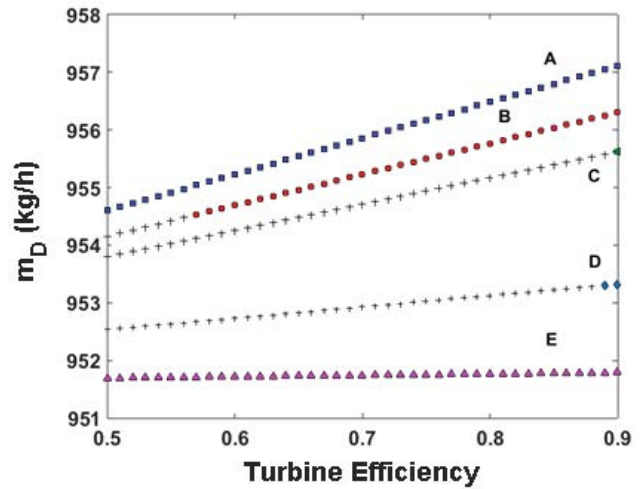


Fig. 12. The impacts of turbine efficiency at different points selected in the Pareto front (Fig. 2) on fresh water production.

Table 3
System parameters in the final optimum point shown in the Fig. 2

Parameters	Value in the optimum final point
Nominal capacity of diesel engine (kW)	50.0011
Partial load	70.0224
Turbine pressure (kPa)	440.0918
Condenser pressure (kPa)	198.4867
ORC mass flow rate (kg/s)	1.1814
Turbine efficiency (-)	0.8992
Pump efficiency (-)	0.8984
System efficiency (-)	0.3799
Total annual cost (\$/y)	4.0785e+04
Fresh water production (kg/s)	954.67

pressure, a higher mass flow rate of feed water leads to more fresh water, as shown in Fig. 13b. When increasing the condenser pressure, the output power of the vapor turbine decreases, which leads to lower RO performance.

The effects of the feed water temperature on the fresh water production at different vapor turbine pressures were also investigated, as shown in Fig. 14. In fact, the different graph lines in the Fig. 14 are shown in the different ambient temperature and its value is increased in the direction of the arrow.

When increasing of the feed water temperature, the mass flow rate of fresh water increases happened at fixed turbine pressure. When increasing the turbine pressure, the turbine temperature decreases and more power is produced. As a result, the RO recovery ratio increases, which increases the fresh water mass flow rate. Therefore, increasing the mass flow rate of the feed water and the temperature leads to an increase in the mass flow rate of the fresh water produced and the recovery ratio.

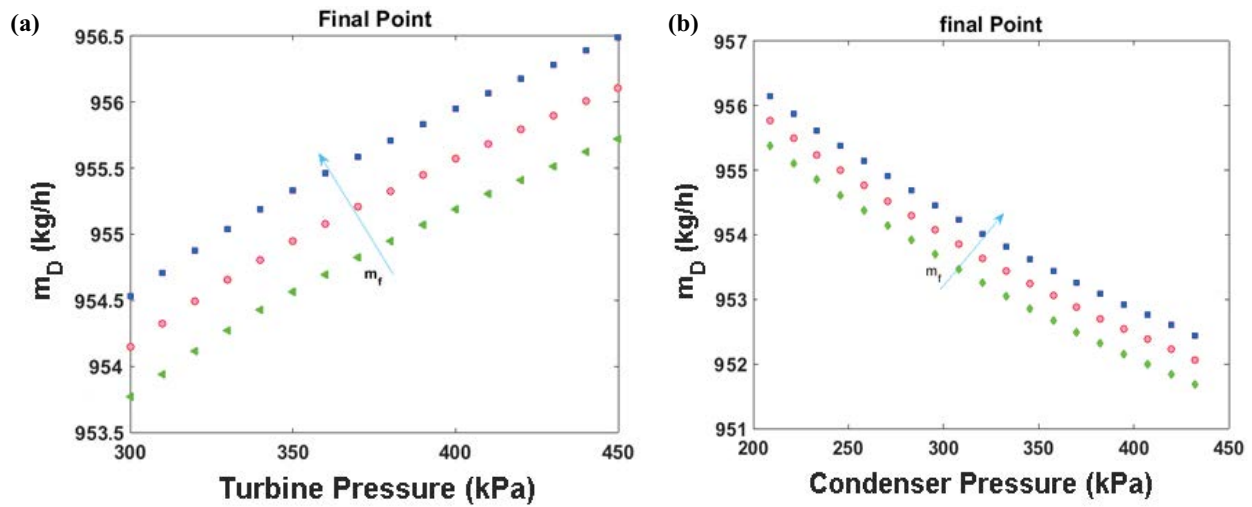


Fig. 13. The effects of feedwater mass flow rate on fresh water production are different: (a) turbine pressure and (b) condenser pressure.

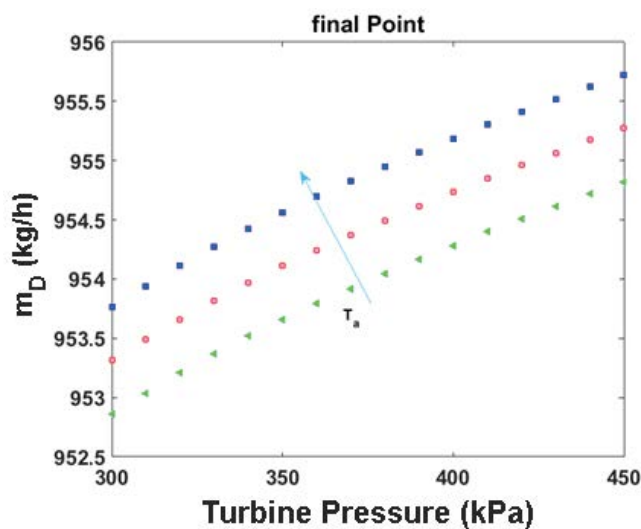


Fig. 14. The effects of ambient temperature on fresh water production at different turbine pressures.

7. Conclusion

This work analyzed a diesel engine-ORC integrated with the RO desalination. The heat wasted from the diesel engine was recovered and supplied to an ORC to generate power in the turbine. This power was used to run a RO unit through a high-pressure pump for the production of fresh water from the seawater. A thermo-economic optimization algorithm was implemented to maximize the power production and consequently the fresh water and decrease the total annual cost. From the optimization results it was concluded that partial load and ORC mass flow rate had the most effect on the trade-off of the objective functions. The design parameters should be selected in the range with higher efficiency at various partial loads since the constraints were violated at lower

values of efficiency. The optimum efficiency obtained to be 37.99% with a TAC of 40,785 \$/y as well as 954.67 kg/s of the fresh water production. The condenser pressure had a negative effect on the fresh water production, while the turbine pressure improved it. The ORC mass flow rate also had a positive effect on the recovery ratio of the RO desalination. At the final optimum point, when increasing the ambient temperature, the fresh water's mass flow rate increased as well. The feed water's mass flow rate enhanced the recovery ratio of the RO and the fresh water's mass flow rate at the final optimum point.

Acknowledgment

This study was supported by the National Research Foundation of Korea (NRF) grant, which is funded by the Korean government (MSIT) (No. 2020R1A5A8018822).

Symbols

A	—	Surface area, m^2
C_{inv}	—	Investment cost, \$
C_{fuel}	—	Fuel cost, \$/y
C_{em}	—	Emission cost, \$/y
D	—	Distilled
F	—	Correction factor
h	—	Specific enthalpy, kJ/kg
ir	—	Interest rate, —
k	—	Heat conduction coefficient
LHV	—	Lower heating value, kJ/kg
\dot{m}	—	Flow rate, kg/s
n	—	System life time
P	—	Pressure, bar
RR	—	Recovery ratio
S_p	—	Membrane salt passage
S_r	—	Salt rejection
T	—	Temperature, K
TDS	—	Total dissolved solids, mg/L
U	—	Overall heat transfer coefficient

\dot{W}	–	Power, kW
X	–	Mass or salt fraction
TAC	–	Total annual cost, \$/y

Greek

α	–	Annualized factor
β	–	Maintenance factor
Ψ_{em}	–	Emission price, \$/kg
φ_f	–	Unit price of fuel, \$/kg
ΔP	–	Pressure drop, Pa
η	–	Efficiency or effectiveness, –
π_{cave}	–	Average feed osmotic pressure
π_p	–	Osmotic permeate pressure

Subscripts

c	–	Cold
con	–	Condenser
D	–	Diesel engine, desalinated water
f	–	Feed and fuel
h	–	Hot
i	–	Inlet
m	–	Membrane
a	–	Ambient condition
o	–	Outlet
P	–	Pump and product
P	–	Product
RO	–	Reverse osmosis
S	–	Isentropic state and steam
T	–	Turbine

References

- O.N. Igobo, P.A. Davies, Isothermal Organic Rankine Cycle (ORC) driving Reverse Osmosis (RO) desalination: experimental investigation and case study using R245fa working fluid, *Appl. Therm. Eng.*, 136 (2018) 740–746.
- B. Anand, R. Shankar, S. Murugavelh, W. Rivera, K. Midhun Prasad, R. Nagarajan, A review on solar photovoltaic thermal integrated desalination technologies, *Renewable Sustainable Energy Rev.*, 141 (2021) 110787, doi: 10.1016/j.rser.2021.110787.
- M. Abdelgaied, A.E. Kabeel, A.W. Kandeal, H.F. Abosheisha, S.M. Shalaby, H.H. Mofreh, Y. Nuo, W.S. Swellam, Performance assessment of solar PV-driven hybrid HDH-RO desalination system integrated with energy recovery units and solar collectors: theoretical approach, *Energy Convers. Manage.*, 239 (2021) 114215, doi: 10.1016/j.enconman.2021.114215.
- N.A. Moharram, B. Seif, A.H. Ahmed, M.E.-M. Wael, Hybrid desalination and power generation plant utilizing multi-stage flash and reverse osmosis driven by parabolic trough collectors, *Case Stud. Therm. Eng.*, 23 (2021) 100807, doi: 10.1016/j.csite.2020.100807.
- A.M. Delgado-Torres, L. García-Rodríguez, Design recommendations for solar organic Rankine cycle (ORC)-powered reverse osmosis (RO) desalination, *Renewable Sustainable Energy Rev.*, 16 (2012) 44–53.
- S. Loutatidou, A.A. Hassan, Techno-economic analysis of MED and RO desalination powered by low-enthalpy geothermal energy, *Desalination*, 365 (2015) 277–292.
- S.K. Karellas, M. Dimitris, K. Terzis, Investigation of an autonomous hybrid solar thermal ORC–PV RO desalination system. The Chalki island case, *Renewable Energy*, 36 (2011) 583–590.
- D. Manolakos, G. Kosmadakis, S. Kyritsis, G. Papadakis, Identification of behaviour and evaluation of performance of small scale, low-temperature Organic Rankine Cycle system coupled with a RO desalination unit, *Energy*, 34 (2009) 767–774.
- S.M. Shalaby, Reverse osmosis desalination powered by photovoltaic and solar Rankine cycle power systems: a review, *Renewable Sustainable Energy Rev.*, 73 (2017) 789–797.
- M. Delgado-Torres, M. Agustín, L. García-Rodríguez, Preliminary design of seawater and brackish water reverse osmosis desalination systems driven by low-temperature solar organic Rankine cycles (ORC), *Energy Convers. Manage.*, 51 (2010) 2913–2920.
- D. Geng, Y. Du, R.-L. Yang, Performance analysis of an organic Rankine cycle for a reverse osmosis desalination system using zeotropic mixtures, *Desalination*, 381 (2016) 38–46.
- A. Nemati, M. Sadeghi, M. Yari, Exergoeconomic analysis and multi-objective optimization of a marine engine waste heat driven RO desalination system integrated with an organic Rankine cycle using zeotropic working fluid, *Desalination*, 422 (2017) 113–123.
- M. Ibarra, A. Rovira, D.C. Alarcón-Padilla, G. Zaragoza, J. Blanco, Performance of a 5 kW_e solar-only organic Rankine unit coupled to a reverse osmosis plant, *Energy Procedia*, 49 (2014) 2251–2260.
- S. Osamah, I. Dincer, Examination of a new solar-based integrated system for desalination, electricity generation and hydrogen production, *Solar Energy*, 163 (2018) 224–234.
- G.H. Xia, Q.X. Sun, J.F. Wang, X. Cao, Y.Z. Yu, L.S. Wang, Theoretical analysis of a reverse osmosis desalination system driven by solar-powered organic Rankine cycle and wind energy, *Desal. Water Treat.*, 53 (2015) 876–886.
- I.E. Ghoujdi, H. Hadiannasab, M. Bidi, A. Naeimi, M.H. Ahmadi, M.A. Nazari, T. Ming, Multiobjective optimization design of the solar field and reverse osmosis system with preheating feed water using Genetic algorithm, *Energy Sci. Eng.*, 6 (2018) 624–642.
- M. Carlos, Y. Bicer, Integrated system based on solar chimney and wind energy for hybrid desalination via reverse osmosis and multi-stage flash with brine recovery, *Sustainable Energy Technol. Assess.*, 44 (2021) 101080, doi: 10.1016/j.seta.2021.101080.
- A. Naseri, B. Mokhtar, H.A. Mohammad, Thermodynamic and exergy analysis of a hydrogen and permeate water production process by a solar-driven transcritical CO₂ power cycle with liquefied natural gas heat sink, *Renewable Energy*, 113 (2017) 1215–1228.
- A. Naseri, B. Mokhtar, H.A. Mohammad, R. Saidur, Exergy analysis of a hydrogen and water production process by a solar-driven transcritical CO₂ power cycle with stirling engine, *J. Cleaner Prod.*, 158 (2017) 165–181.
- Z. Hajabdollahi, K.C. Kim, Thermo-economic modeling and multi-objective optimization of multiple-effect desalination integrated with an organic Rankine cycle, *Desal. Water Treat.*, 152 (2019) 148–160.
- H. Ansarinasab, H. Hajabdollahi, M. Fatimah, Life cycle assessment (LCA) of a novel geothermal-based multigeneration system using LNG cold energy-integration of Kalina cycle, stirling engine, desalination unit and magnetic refrigeration system, *Energy*, 231 (2021) 120888, doi: 10.1016/j.energy.2021.120888.
- V. Ghamari, H. Hajabdollahi, M. Shafiey Dehaj, Comparison of gas turbine and diesel engine in optimal design of CCHP plant integrated with multi-effect and reverse osmosis desalinations, *Process Saf. Environ. Prot.*, (2021) (in Press), doi: 10.1016/j.psep.2021.07.030.
- A.S. Nafey, M.A. Sharaf, L. García-Rodríguez, Thermo-economic analysis of a combined solar organic Rankine cycle-reverse osmosis desalination process with different energy recovery configurations, *Desalination*, 261 (2010) 138–147.
- A. Altaee, Computational model for estimating reverse osmosis system design and performance: part-one binary feed solution, *Desalination*, 291 (2012) 101–105.
- Handbook A. “Chapter S7” Cogeneration Systems and Engine and Turbine Drives, 1999, pp. 7–46.

- [26] Z. Hajabdollahi, F. Hajabdollahi, M. Tehrani, H. Hajabdollahi, Thermo-economic environmental optimization of Organic Rankine Cycle for diesel waste heat recovery, *Energy*, 63 (2013) 142–151.
- [27] Z. Hajabdollahi, H. Hajabdollahi, P.F. Fu, The effect of using different types of nanoparticles on optimal design of fin and tube heat exchanger, *Asia-Pac. J. Chem. Eng.*, 12 (2017) 905–918.
- [28] Z. Hajabdollahi, H. Hajabdollahi, K.C. Kim, Heat transfer enhancement and optimization of a tube fitted with twisted tape in a fin-and-tube heat exchanger, *J. Therm. Anal. Calorim.*, 140 (2020) 1015–1027.
- [29] P-L. Yu, *Multiple-Criteria Decision Making: Concepts, Techniques, and Extensions*, Springer Science & Business Media, 2013.